Alexander Grahn[1]
e-mail: a.grahn@fzd.de

Eckhard Krepper

Frank-Peter Weiß

Institut für Sicherheitsforschung,
Forschungszentrum Dresden-Rossendorf e. V.,
01314 Dresden, Germany

Sören Alt

Wolfgang Kästner

Alexander Kratzsch

Rainer Hampel

Institut für Prozesstechnik,
Prozessautomatisierung und Messtechnik,
Hochschule Zittau-Görlitz,
University of Applied Sciences,
02754 Zittau, Germany

Implementation of a Pressure Drop Model for the CFD Simulation of Clogged Containment Sump Strainers

The present study aims at modeling the pressure drop of flows through growing cakes of compressible fibrous materials, which may form on the upstream side of containment sump strainers after a loss-of-coolant accident. The model developed is based on the coupled solution of a differential equation for the change of the pressure drop in terms of superficial liquid velocity and local porosity of the fiber cake and a material equation that accounts for the compaction pressure dependent cake porosity. Details of its implementation into a general-purpose three-dimensional computational fluid dynamics code are given. An extension to this basic model is presented, which simulates the time dependent clogging of the fiber cake due to capturing of suspended particles as they pass trough the cake. The extended model relies on empirical relations, which model the change of pressure drop and removal efficiency in terms of particle deposit in the fiber cake.
[DOI: 10.1115/1.4000365]

1 Introduction

The investigation of insulation debris generation and transport during loss-of-coolant accident (LOCA) events, as well as the short and long term behavior of the emergency core cooling system (ECCS) must be considered with regard to the safety of pressure and boiling water reactors under such conditions [1–3]. The mineral wool blankets that are used to insulate the components of nuclear reactors can be destroyed by jetting steam during LOCA. A portion of the mineral wool fiber debris can then be transported into the containment sump, which collects the cooling water for use in the ECCS in the late phase of LOCA. Mineral wool fibers that accumulate at the ECCS pump suction strainers lead to increased pressure drops, which could reduce the pumps capability to recirculate the cooling water. Hazards associated with such an incident were emphasized by an incident at the Barsebäck-2 nuclear power plant in Sweden in 1992 when a steam valve inadvertently opened [4]. The debris quickly blocked the ECCS pump strainers, resulting in a potential compromise in the defense-in-depth concept for the reactor.

The transient build-up of the pressure drop after LOCA can be divided into two different stages. The first, significant increase in the pressure drop occurs soon after the LOCA event and results from accumulation of the fibrous particles originating from the destroyed insulation blankets in the neighborhood of the break. Due to the size of the insulation fibers, only a little quantity of them is able to penetrate the sump strainers, which are usually made of perforated plates with holes measuring a few millimeters in diameter. Most fibers reaching the strainer immediately form a highly compressible cake of high porosity. This cake is an effective means of removing the remaining fibers suspended in the coolant. In the later stage of the LOCA, a second strong increase in the pressure drop may occur in spite of an apparently clear coolant flow. This effect has attracted the attention of nuclear regulatory commissions as it may severely undermine the long-term reliability of the ECCS [5]. It is attributed to fine grained particles and hydrated gels, which are trapped on the fiber surfaces in the interior of the fiber cake. The deposit increases the roughness of fiber surfaces and constricts the free cross section available to the flow. Chemical interactions in the post-LOCA phase between the ECCS water, which contains boric acid and sodium hydroxide at elevated temperatures, and exposed metal surfaces, paint coatings or insulation debris are supposed to be the source of the deposit.

This study proposes a model for calculating the transient build-up of the pressure drop over a growing, compressible fibrous bed. This basic model has been implemented into the commercial, general-purpose computational fluid dynamics (CFD) code ANSYS-CFX [6] in order to calculate the pressure drop at nonuniformly loaded strainers. The subsequent clogging of the fiber cake by suspended fine particles is addressed in a generic way by treating the cake as a depth filtration medium, which is subject to a coolant flow with a given concentration of particles impinging on its upstream end. This extended model should be considered as a first approach to the problem of ECCS long-term effects as it currently relies on empirical formulations of correction functions for the deposit dependent pressure drop and filtration efficiency. These correction functions have yet to be adjusted to experiments.

2 Theoretical Model

The initial stage after activation of the ECCS pumps is marked by the accumulation of fibrous particles on the upstream side of the containment sump strainers. At this time, the coolant is essentially free of secondary debris, i.e., of fine particles stemming from corrosion and other chemical effects, and the cake forming on the upstream side of the strainers remains clean. Due to the deformability of the fibers, the cake can be easily compressed under the action of fluid drag forces or an external compacting pressure. The basic model describing the flow through compressible clean fiber beds is presented in the following Sec. 2.1. The

[1]Corresponding author.

Contributed by the Nuclear Division of ASME for publication in the JOURNAL OF ENGINEERING FOR GAS TURBINES AND POWER. Manuscript received July 22, 2009; final manuscript received August 19, 2009; published online May 28, 2010. Editor: Dilip R. Ballal.

Copyright © 2010 by ASME

Downloaded 02 Jun 2010 to 171.66.16.96. Redistribution subject to ASME license or copyright; see http://www.asme.org/terms/Terms_Use.cfm

flow of fine particle loaded coolant trough fiber beds involves the solution of additional transport and balance equations to get the distribution of particles deposited in the fiber cake. The necessary model extension for this type of flow is presented in Sec. 2.2.

2.1 Flow Through Clean Fibrous Bed. A standard approach in the investigation of fluid flow in macroscopically homogeneous porous medium is to characterize the system in terms of Darcy's law

$$U = -\frac{k}{\mu}\frac{\Delta p}{L} \tag{1}$$

It linearly relates the superficial flow velocity U to the hydraulic pressure difference Δp that is applied to a layer of porous material of streamwise thickness L and permeability k; μ is the dynamic viscosity of the fluid. However, as evidenced by numerous experiments, this relationship only holds for very low flow velocities where viscous forces predominate. Unlike pipe flow, which is characterized by a sudden passage from the viscous to the inertial regime at a critical Reynolds number, the departure from the linear $U \sim \Delta p$ relationship proves to be gradual for flow in porous media. Consequently, the contribution of inertia to the flow in the pore space should also be examined in the framework of the laminar flow regime before assuming that fully developed turbulence effects are present and relevant to momentum transport [7].

A more general relationship between flow velocity and pressure drop is given by the Forchheimer equation [8]

$$\frac{\Delta p}{L} = -(\alpha\mu U + \beta\rho U^2) \tag{2}$$

It regards the flow resistance of a porous layer as being made up of two parts. The first one, which results from viscous forces, depends linearly on velocity, while the second one, resulting from inertial effects, is proportional to density ρ of the liquid phase times the square of velocity. The relative importance of both parts is weighted by empirical coefficients α and β. Note that Eq. (2) is not purely empirical, since it can be derived by an appropriate average of the Navier–Stokes equation for one-dimensional steady incompressible laminar flow of a Newtonian fluid in an incompressible porous medium [8].

Initial efforts, dating back to the 1930s, focused on the determination of the coefficient α of Eq. (2) for purely viscous flow within porous media. They lead to the well-known Carman–Koženy equation [9]

$$\frac{\Delta p}{L} = -\frac{k(A_f\rho_f)^2(1-\varepsilon)^2}{\varepsilon^3}\mu U \tag{3}$$

where A_f is the surface area per unit mass of the particle phase, ρ_f is its material density, and k is the Koženy constant, a to-be-determined empirical coefficient; porosity ε is defined as

$$\varepsilon = \frac{V_v}{V_{\text{tot}}} \tag{4}$$

and expresses the ratio between the void (=pore) volume V_v and the total volume V_{tot} of the porous bed. Equation (3) has been extensively used in connection with granular media; it has shown to yield bad results for fibrous media, though. Analytical reasoning for this is given in Ref. [10]. For fiber structures Davies [11] proposed the equation

$$\frac{\Delta p}{L} = -a(A_f\rho_f)^2(1-\varepsilon)^{1.5}[1 + a_0(1-\varepsilon)^3]\mu U \tag{5}$$

which showed better agreement with measured pressure drops over fibrous beds at laminar flow conditions. Based on a large amount of experimental data, Ingmanson et al. [12] found values of 3.5 and 57 for the empirical coefficients a and a_0. To date these constants have been widely used for laminar flow through fibrous porous media. However, as will be shown later, different values of these coefficients have been determined for mineral wool fibers.

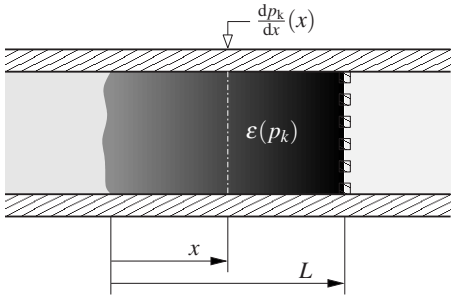

Fig. 1 Fiber cake at a strainer

Davis' equation still neglects the contribution of inertia to the over-all pressure drop of flow in the pore space. This deficiency was remedied by Ergun [13] who suggested the relation

$$\frac{\Delta p}{L} = -b\frac{A_f\rho_f(1-\varepsilon)}{\varepsilon^3}\rho U^2 \tag{6}$$

for the turbulent flow regime in granular media. Nevertheless, experimental studies [10] indicated that the functional relationship in Eq. (6) can as well be applied to turbulent flow in fibrous media. The empirical constant b was found to be close to 0.66.

Equations (5) and (6) can be combined to give a relation that encompasses the whole range of flow regimes from laminar to turbulent. It reads

$$\frac{\Delta p}{L} = -\left\{a(A_f\rho_f)^2(1-\varepsilon)^{1.5}[1 + a_0(1-\varepsilon)^3]\mu U + b\frac{A_f\rho_f(1-\varepsilon)}{\varepsilon^3}\rho U^2\right\} \tag{7}$$

A simple force balance shows that the mechanical pressure, which acts on the fibers and which results from the fluid drag, increases in the streamwise direction along the cake. As fiber cakes are compressible, this leads to a porosity distribution with a maximum at the upstream and a minimum at the downstream end. Figure 1 illustrates this decrease in porosity by the shading getting darker in the streamwise direction. Therefore, Eq. (7) can only be used to calculate the *differential* change of the pressure drop $d(\Delta p)/dx$ from local porosity values $\varepsilon(x)$. Hence, integration of Eq. (7) in the streamwise direction is required to obtain the total pressure drop Δp over the fiber cake length L.

The local change in compacting pressure dp_k/dx and the pressure drop $d(\Delta p)/dx$ of the flow have the same absolute value but are opposite in sign. For dp_k/dx it follows from Eq. (7)

$$\frac{dp_k}{dx} = -\frac{d(\Delta p)}{dx} = a(A_f\rho_f)^2(1-\varepsilon)^{1.5}[1 + a_0(1-\varepsilon)^3]\mu U + b\frac{A_f\rho_f(1-\varepsilon)}{\varepsilon^3}\rho U^2 \tag{8}$$

As indicated above, the cake porosity depends on the local compacting pressure. Hence, the complete description of the flow still requires a compressibility function that relates porosity ε to the compacting pressure p_k. The volume reduction in a porous bed subject to a compacting pressure results from deformation of the solids. Generally, the volume reduction is, in part, irreversible because portions of the particles that constitute the bed may disintegrate or change their mutual orientation within the solid matrix. To the author's knowledge, a complete theoretical foundation of the irreversible compression of porous media has not yet been published. One possible method to workaround this problem is to use different expressions for the first and the subsequent compressions of the porous bed, as shown in Ref. [14], where the solid is

Downloaded 02 Jun 2010 to 171.66.16.96. Redistribution subject to ASME license or copyright; see http://www.asme.org/terms/Terms_Use.cfm

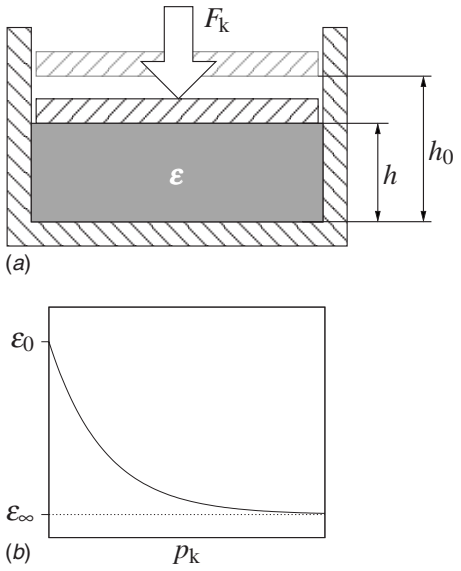

Fig. 2 (*a*) compaction measurement principle; (*b*) typical compaction curve $\varepsilon(p_k)$

regarded as mechanically conditioned after the first compression, that is, having a constant compressibility independent of the compacting pressure.

The present study considers the flow through a growing bed of fibers, which are deposited from a dilute fiber suspension during LOCA. Thus, the change of material properties due to repeated compression and release plays a secondary role and shall be neglected here. It should be pointed out, however, that the latter assumption does not imply a restriction of the applicability of the flow equation presented here as it can be combined with any working compressibility function.

For a given fibrous material the compressibility function must be determined experimentally. The measurement principle is depicted in Fig. 2(*a*). A known quantity m_f of insulation material, placed into a vertical cylinder with cross-sectional area A, is subject to a uniform compacting pressure p_k, resulting from an externally applied force F_k. Then, p_k amounts to

$$p_k = \frac{F_k}{A} \tag{9}$$

and porosity ε can be calculated from height h as

$$\varepsilon = 1 - \frac{m_f}{\rho_f A h} \tag{10}$$

Most compressibility functions for fibrous beds, relating bed porosity ε to mechanical compacting pressure p_k, have the form [15]

$$\varepsilon = 1 - q p_k^r \tag{11}$$

with empirical parameters q and r. This expression, however, suffers from the fact that it does not give adequate estimates for the limiting cases of zero and infinite compaction pressures. Therefore, the four-parameter equation

$$\varepsilon(p_k) = \varepsilon_\infty + (\varepsilon_0 - \varepsilon_\infty) e^{-C p_k^D} \tag{12}$$

is suggested, which does not have this shortcoming. It has proven to reproduce measured relationships $\varepsilon(p_k)$ especially well. Figure 2(*b*) illustrates the expected curve, as well as two of the parameters, the porosities ε_0 and ε_∞ at zero and infinite compacting pressures. Determination of the parameters in Eq. (12) requires a nonlinear least-squares fitting method, such as the Marquardt–Levenberg algorithm, which is, for example, implemented in the

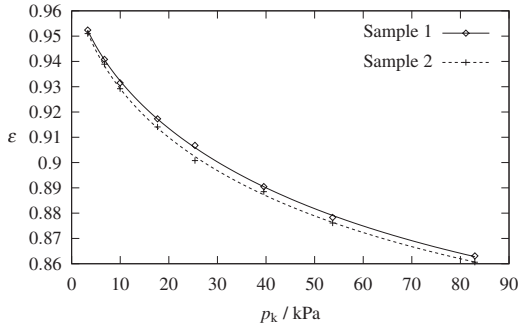

Fig. 3 Measured relationship of compaction pressure p_k and porosity ε for given samples of mineral wool

open-source data plotting software GNUPLOT [16].

Figure 3 shows compaction measurements (points) and their approximation by Eq. (12) (lines) of two different mineral wool samples. Measurements were performed at room temperature as the elastic properties of the mineral fibers are supposed not to change significantly in the expected range of temperatures below 100°C. The material density ρ_f, which is needed to calculate the porosity ε, Eq. (10), was measured by helium pycnometry (PENTAPYCNOMETER V. 2.1, Quantachrome Instruments, Boynton Beach, FL, USA). Densities and compaction parameters of the rock wool samples are summarized in Table 1.

Flow equation (8) and compressibility function (12) constitute an initial value problem for calculating the streamwise compaction pressure and porosity profiles along the fiber cake. It has to be solved by integration with respect to x starting at the upstream end of the cake toward the strainer plate with initial conditions $p_k(0) = 0$ and $\varepsilon(0) = \varepsilon_0$, which correspond to zero compaction pressure and standard porosity of the mineral wool.

A stopping condition for the integration needs to be formulated yet. Integration should stop as soon as the amount of fibrous phase contained in the integration interval corresponds to a previously given strainer mass load $N_{f,\text{given}}$. In the case of a growing fiber cake, this mass load may be obtained by integrating the suspended fibers mass flow rate with respect to time. Strainer mass load N_f is defined as mass of fibers per unit area of strainer plate. The contribution dN_f of an infinitesimal slice dx of the cake to the total strainer mass load is calculated from local porosity ε as

$$dN_f = \rho_f (1 - \varepsilon) dx \tag{13}$$

Thus, differential equation

$$\frac{dN_f}{dx} = \rho_f (1 - \varepsilon) \tag{14}$$

must be solved together with the differential equation of flow (8), subject to the initial condition $N_f = 0$ at the upstream end of the cake. Integration stops on fulfilling the condition $N_f(x) = N_{f,\text{given}}$, yielding the total length (streamwise thickness) L of the compressed fiber cake. The pressure difference over the entire fiber bed follows directly from the compacting pressure at the strainer position as

$$\Delta p = - p_k(L) \tag{15}$$

Table 1 Material density and compaction parameters of mineral wool samples

	ρ_f (kg m^{-3})	ε_0	ε_∞	C (Pa^{-D})	D
Sample 1	2740	0.9744	0.8169	0.00078	0.6502
Sample 2	2690	0.9817	0.8083	0.00195	0.5668

Downloaded 02 Jun 2010 to 171.66.16.96. Redistribution subject to ASME license or copyright; see http://www.asme.org/terms/Terms_Use.cfm

2.2 Clogging of the Fiber Bed by Solid Particles. In the late phase of a LOCA, when most of the primary fibrous debris have been removed from the coolant flow, the fiber cake acts as a depth filtration medium because small particles, which have been generated by chemical processes in the upstream regions of the containment, such as corrosion and precipitation, penetrate into the cake and deposit at various depths. The filtration process is intrinsically transient, as deposited material changes both the geometry of the interstitial space in the cake and the nature of the collector (fiber) surfaces. This is reflected in the variations in the filter efficiency being a measure of the fiber cake's ability to remove particles from the flow and of the pressure drop.

The particle distribution within a filter bed is governed by a macroscopic mass conservation equation and a rate equation. Under normal filtration conditions, where the suspension flow velocity is in the order of centimeters per second, particles are transported mainly by advection and particle diffusion due to Brownian motion can be neglected. Then, the mass conservation can be written as [17]

$$\frac{d\sigma}{dt} + \frac{d}{dx}(u\zeta_p) = 0 \tag{16}$$

where σ is the volumetric deposit (volume of captured particles per volume of filter bed), u is the suspension approach velocity, and ζ_p is the suspension concentration (particle volume fraction). The rate at which the quantity of captured particles changes with time can be expressed as

$$\frac{d\sigma}{dt} = \lambda u \zeta_p \tag{17}$$

Unlike the mass conservation equation, which is independent of the clogging mechanism, the rate equation, in particular, the filter coefficient λ, is a function of the elementary processes, which are responsible for the transfer of particles from suspension to the immobilized state. Research into the modeling of depth filtration has concentrated on predicting λ from σ, i.e., how the removal efficiency changes as deposition in the filter increases. A number of empirical approaches have been used, see Ref. [18] for an overview. Later in this study we will use some basic relationships to establish the connection between filter coefficient λ and volumetric deposit σ and similarly for the pressure drop.

It is convenient to substitute the suspension approach velocity u by the superficial liquid velocity U, since the latter does not change in the streamwise direction of an axial filter. With $U = u(1-\zeta_p)$ we get from Eq. (16)

$$\frac{d\sigma}{dt} + \frac{U}{(1-\zeta_p)^2}\frac{d\zeta_p}{dx} = 0 \tag{18}$$

and from Eq. (17)

$$\frac{d\sigma}{dt} = \lambda U \frac{\zeta_p}{1-\zeta_p} \tag{19}$$

Equations (18) and (19) can be combined and solved for $d\zeta_p/dx$ giving

$$\frac{d\zeta_p}{dx} = -\lambda \zeta_p (1-\zeta_p) \tag{20}$$

This is a first order ordinary differential equation for the suspension concentration ζ_p within the fiber cake. It must be integrated along x with the influent suspension concentration as initial condition for ζ_p at the upstream end of the fiber cake.

As stated above, the filter coefficient λ is a function of the amount of deposited particles σ and of the clean fiber cake porosity ε. This can be expressed as

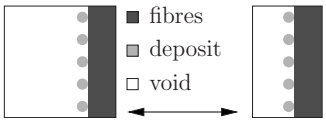

Fig. 4 Clogged fiber bed element in uncompressed and compressed states

$$\lambda = F_1(\sigma,\varepsilon)\lambda_c(\varepsilon) \tag{21}$$

where λ_c is the porosity dependent clean bed filter coefficient and F_1 is a correction factor, which accounts for the altered collecting ability of the clogged cake. F_1 also depends on the cake porosity. Likewise, the pressure drop of a clogged filter is different from a clean one. As the pressure drop Δp is equivalent to the compaction pressure p_k, one writes

$$\frac{dp_k}{dx} = F_2(\sigma,\varepsilon)\left(\frac{dp_k}{dx}\right)_c \tag{22}$$

in order to correct the compaction pressure, which is obtained for the clean fiber bed by integrating Eq. (8). It can be anticipated that F_1 and F_2, as well as λ_c, are complicated functions owing to the difficult nature of the particle fiber interaction. The deposit distribution σ in the cake required by F_1 and F_2 is obtained by integrating Eq. (19) with respect to time.

While the deposit quantity grows in the fiber cake, the cake structure changes and hence its permeability to the flow decreases. Obviously, this clogging process is not uniform throughout the cake, but advances in the direction of the main flow. Although clogging starts at the upstream end of the cake, the increased pressure drop there contributes to the compaction of the deeper cake sections, even if the latter has not yet been reached by the suspension. This leads to a further compression of the entire cake, reducing its length L. As stated above, to get the deposit distribution in the cake at a particular time it is necessary to integrate Eq. (19) between the start of clogging, i.e., the moment when suspension reaches the upstream end of the cake, and that time. Since a numerical scheme is to be adopted to solve the set of coupled differential equations, the deposit distribution at previous time steps must be held in computer memory. In view of a variable fiber bed length L, it is therefore necessary to map the deposit values σ at position x along the compressed bed onto values σ' at positions x' of the uncompressed bed.

Based on the volume of deposited particles V_p and the total volume of the cake element V_{tot}, the volumetric deposit σ is defined as

$$\sigma = \frac{V_p}{V_{\text{tot}}} \tag{23}$$

V_{tot} can be expressed in terms of the clean bed porosity ε and the volume of fibers V_f

$$V_{\text{tot}} = \frac{V_f}{1-\varepsilon} \tag{24}$$

Substitution into Eq. (23) gives

$$\sigma = \frac{V_p}{V_f}(1-\varepsilon) \tag{25}$$

From Fig. 4 it can be concluded that the ratio between the deposited particle volume V_p and the volume of fibers V_f remains constant if a cake element undergoes compression. Thus

$$\frac{V_p}{V_f} = \frac{\sigma}{1-\varepsilon} = \text{const} \tag{26}$$

and the volumetric deposits of an uncompressed and a compressed cake element relate as

Downloaded 02 Jun 2010 to 171.66.16.96. Redistribution subject to ASME license or copyright; see http://www.asme.org/terms/Terms_Use.cfm

$$\frac{\sigma'}{\sigma} = \frac{1-\varepsilon_0}{1-\varepsilon} \tag{27}$$

Equation (27) can be used to convert forth and back between compressed and uncompressed bed deposit values σ and σ'.

A mapping function between the streamwise coordinates x' and x of an uncompressed and a compressed bed can be derived from Eq. (13). For an uncompressed bed one can similarly write

$$dN_f = \rho_f(1-\varepsilon_0)dx' \tag{28}$$

Now, the amount of fibers dN_f contained in the infinitesimal slices dx of a compressed bed and dx' of an uncompressed bed should be the same such that Eqs. (13) and (28) can be combined to the ordinary differential equation

$$\frac{dx'}{dx} = \frac{1-\varepsilon(x)}{1-\varepsilon_0} \tag{29}$$

It allows one to calculate the uncompressed bed position x' belonging to the compressed bed position x.

For the solution of Eq. (20) we still need the time dependent penetration depth x_{pen} of the suspension because ζ_p, which appears on the right hand side of the differential equation must be set to zero when integration along x goes past x_{pen}. At time t, the volume of suspension that has entered the fiber cake so far amounts to

$$V_s = A\int_0^t u d\tau = A\int_0^t \frac{U}{1-\zeta_{p,\text{up}}} d\tau \tag{30}$$

where $\zeta_{p,\text{up}}$ designates the particle suspension concentration at the upstream end of the fiber bed and A is the bed cross-sectional area. This corresponds to the void (interfiber) volume

$$V_v = \varepsilon_0 A x'_{\text{pen}} \tag{31}$$

of an uncompressed clean fiber bed filled with suspension up to x'_{pen}. Thus, while integrating Eqs. (20) and (29), ζ_p is to be set to zero as soon as

$$x' > \frac{1}{\varepsilon_0}\int_0^t \frac{U}{1-\zeta_{p,\text{up}}} d\tau \tag{32}$$

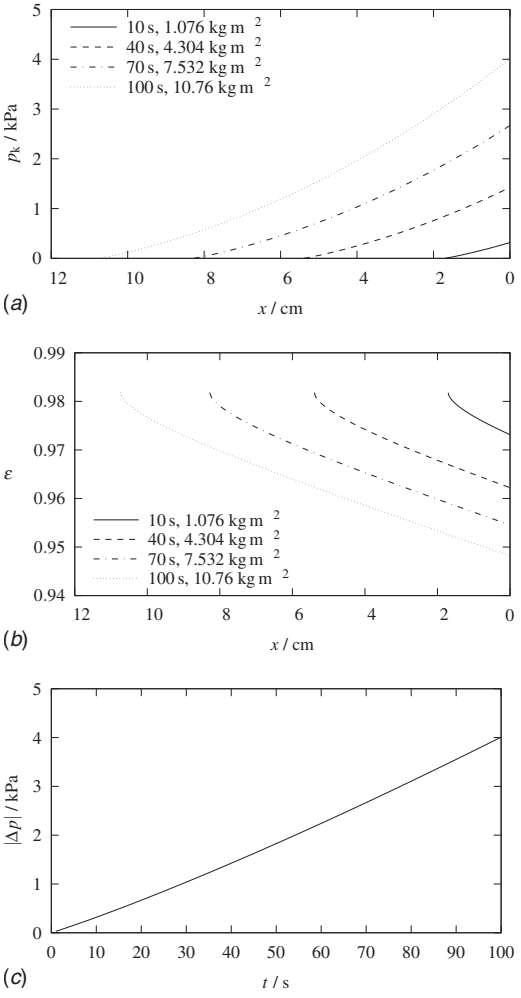

Fig. 5 Fiber cake build-up; profiles of (*a*) compaction pressure, (*b*) porosity; (*c*) development of pressure drop; $u = 4$ cm s^{-1}, $\zeta_f = 0.001$

3 Application of the Model Equations

First, the application of the model equations to the case of a clean compressible fiber cake, which is formed during the first phase of a LOCA, will be demonstrated. The initial value problem consisting of Eqs. (8) and (14) is integrated numerically by means of the differential equation solver LSODAR from the open-source library ODEPACK [19]. The local porosity ε is calculated from the local compaction pressure p_k using material Eq. (12).

Equation (8) contains empirical parameters a, a_0, and b, which must be determined by experiment. As the mass specific surface A_f of the fibrous material is difficult to be measured, empirical parameters a and b, and the material properties A_f and ρ_f were combined to

$$\tilde{a} = a(A_f\rho_f)^2 \quad \text{and} \quad \tilde{b} = bA_f\rho_f \tag{33}$$

From pressure drop measurements the values $\tilde{a} = 1.1275 \times 10^{11}$ m^{-2}, $a_0 = 120$, and $\tilde{b} = 5.8089 \times 10^4$ m^{-1} were found for mineral wool sample 2 (cf. Table 1).

Calculated profiles of compaction pressure and cake porosity in a growing fiber cake are shown in Figs. 5(*a*) and 5(*b*). The left end x positions of the profiles mark the total length L of the compressed fiber bed, while $x=0$ marks the strainer position. For constant flow velocity u and upstream fiber concentration ζ_f, the shape of the profiles does not change with time but is shifted to the left as the cake grows. The nonlinearity of the pressure profiles is caused by the compressibility of the cake. Cake porosity ε decreases in the flow direction due to the growing compaction pressure and hence dp_k/dx increases because it depends on ε. The pressure drop over the cake, as shown in Fig. 5(*c*), increases slightly progressively with time since the mean porosity of the growing cake decreases.

Figure 6 shows the compaction pressure and porosity profiles in a cake of constant mass, where the flow velocity of the liquid has been varied. The cake length decreases as the velocity increases and the nonlinearity of profiles becomes more pronounced.

The pressure drop Δp over the fiber cake was determined, both numerically and experimentally, as a function of the superficial velocity for different water temperatures. A schematic view of the experimental set-up is given in Fig. 7. Results are shown in Fig. 8. The measurement at $T = 70\,^\circ$C was used to determine the material specific model parameters $\tilde{a}$, $\tilde{b}$, Eq. (33), and a_0, which were then used in subsequent calculations with different mass loads and temperatures. For comparison the computed curves and measured data points have been plotted into one diagram. Pressure drops measured at different experimental conditions could be reproduced with reasonable accuracy. A small offset between the experimental and calculated curves is due to an offset in the measurement which produced nonzero Δp values at zero flow velocity.

The clogging of a fiber cake of constant fiber mass load subject to a fine particle suspension flow was simulated based on the extended model. Differential Eqs. (20), (22), and (29) are solved

Downloaded 02 Jun 2010 to 171.66.16.96. Redistribution subject to ASME license or copyright; see http://www.asme.org/terms/Terms_Use.cfm

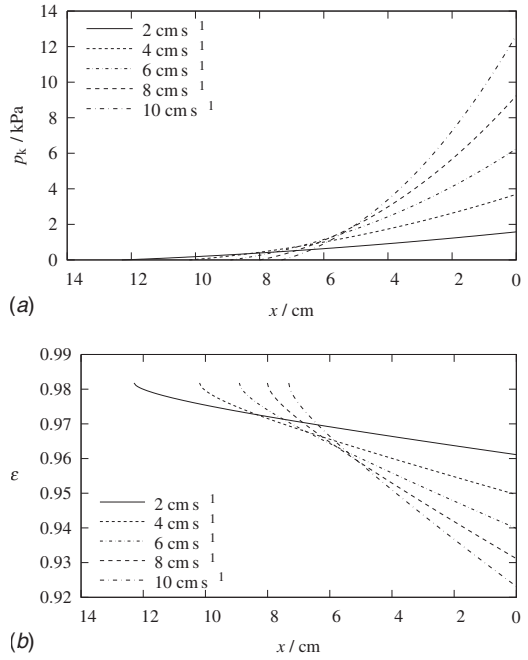

Fig. 6 Profiles of (*a*) compaction pressure and (*b*) porosity at given strainer mass load (N_f=10 kg m^{-2}) for different superficial velocities *U*

numerically by means of the solver LSODAR, and Eq. (19) was integrated with respect to time using the Euler method of first order with a constant timestep of Δt=0.01 s. The deposit concentration σ is assumed to be small such that the elastic properties of the fiber cake are unaffected and the parameters in Eq. (12) remain constant.

As stated above, the interaction between particles and the grain or fiber surfaces of filter media is still far from being completely understood. Hence, many correlations, most of them empirical, exist in the literature [20]. The empirical ones usually calculate correction factors that are multiplied with the filter coefficient λ_c and the pressure drop $(\Delta p)_c$ of the clean filter media

$$\lambda = F_1(\sigma)\lambda_c \tag{34a}$$

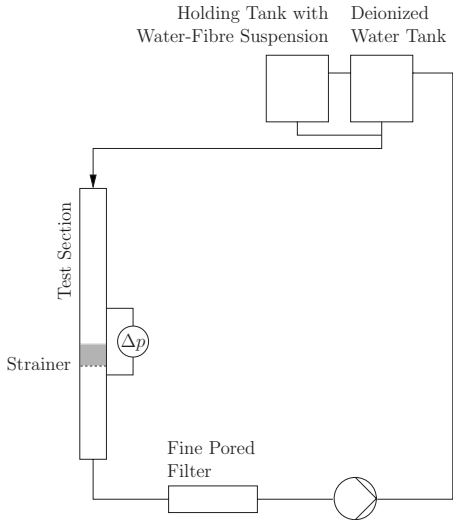

Fig. 7 Test rig for pressure drop measurements

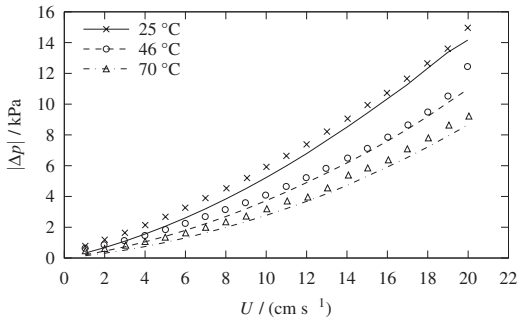

Fig. 8 Calculated and experimentally determined pressure drop-superficial velocity relationship at different temperatures, N_f=5.41 kg m^{-2}

$$\Delta p = F_2(\sigma)(\Delta p)_c \tag{34b}$$

Since we are dealing with compressible filter media, it is most probable that the clean filter coefficient λ_c is a function of ε, as a particle is more likely to be captured by a filter whose fibers are packed more densely. Therefore, the simple relation

$$\lambda_c(\varepsilon) = -b_\lambda \ln \varepsilon \tag{35}$$

will be used here to make λ_c depend on the clean bed porosity. b_λ is an empirical parameter to be obtained from experiments. Equation (35) evaluates to zero at ε=1 (no fibers) and tends to infinity as ε approaches zero (no void).

Often, the corrections F_1 and F_2 in Eq. (34) have the form

$$F_1(\sigma) = 1 + b_{F1}\sigma \tag{36a}$$

$$F_2(\sigma) = 1 + b_{F2}\sigma \tag{36b}$$

with b_{F1} and b_{F2} being empirical constants. Although related to the fiber cake volume, the volumetric deposit σ serves here as a measure of the degree of fouling of the fibers by captured particles. If the filter is incompressible, this is equivalent to relating the captured particle volume to the fiber volume because the ratio between fibers and total cake volume is constant. However, if the cake is compressible, it would be more appropriate to use the ratio V_p/V_f instead of σ as a fouling measure in the correction functions because V_p/V_f is independent of the fiber cake's compression state (cf. Fig. 4). Replacing σ by V_p/V_f in Eq. (35) and making use of Eq. (26) gives

$$F_1(\sigma,\varepsilon) = 1 + b_{F1}\frac{\sigma}{1-\varepsilon} \tag{37a}$$

$$F_2(\sigma,\varepsilon) = 1 + b_{F2}\frac{\sigma}{1-\varepsilon} \tag{37b}$$

which will be used as correction factors in Eqs. (21) and (22) introduced above.

The ability of the extended model to calculate the clogging process of a fiber cake is demonstrated in Fig. 9. The present case is based on arbitrarily chosen parameter values in Eqs. (35) and (37). Experiments are needed to provide more realistic values. Although the clean fiber mass load N_f and the flow velocity U are held constant, compaction pressure, Fig. 9(*a*), and porosity profiles, Fig. 9(*b*), get steeper with time due to the increasing flow resistance of the clogging cake. As a consequence, the cake is further compacted and the total bed length L decreases. Suspension concentration profiles are shown in Fig. 9(*c*). The steep drop in the concentration profile at t=4 s marks the propagating concentration front, which separates the penetrating particle suspension from the clear water being displaced from the cake. Since a

Downloaded 02 Jun 2010 to 171.66.16.96. Redistribution subject to ASME license or copyright; see http://www.asme.org/terms/Terms_Use.cfm

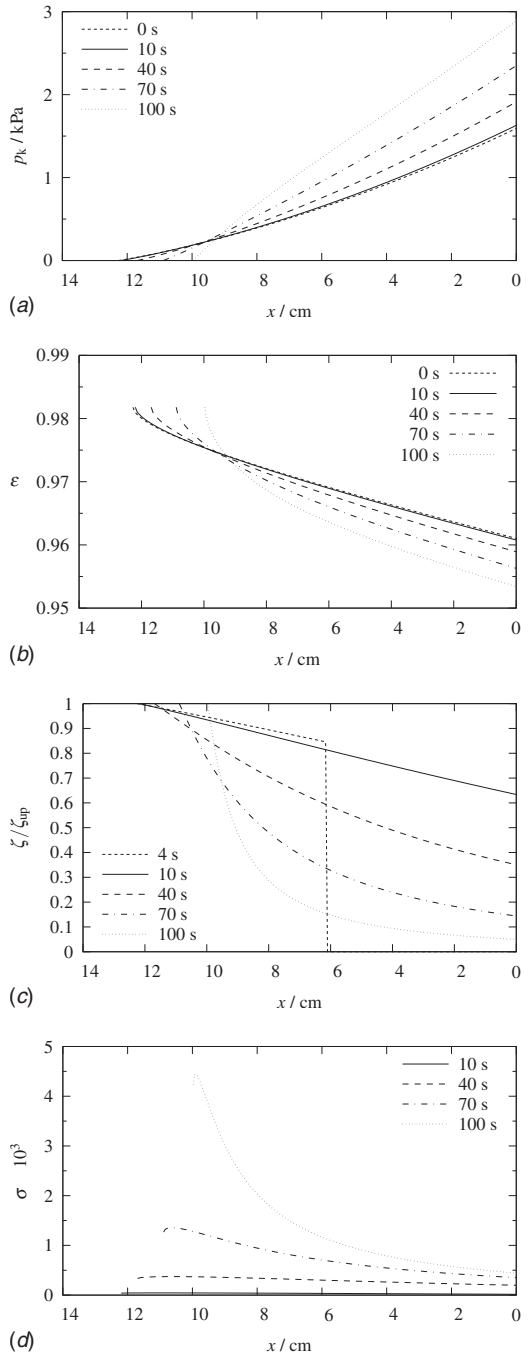

Fig. 9 Fiber cake clogging; profiles of (*a*) compaction pressure, (*b*) porosity, (*c*) suspended particle concentration, and (*d*) specific deposit; $U=2$ cm s^{-1}, $N_f=10$ kg m^{-2}, $\zeta_{p,up}=0.0001$, $b_\lambda=100$, $b_{F1}=200$, and $b_{F2}=20$

positive value has been chosen for b_{F1}, the filter performance of the cake enhances with growing deposit concentration and the effluent particle concentration at $x=0$ decreases with time. In reality, however, the $\lambda-\sigma$ relationship is not monotonic, and one distinguishes several stages of the filtration process with an initial increase and a subsequent decrease in the filter coefficient [21]. More advanced correlations than Eqs. (35) and (37) should therefore be used for practical applications. Finally, the deposit distributions are plotted in Fig. 9(*d*). It can be seen that the current set of parameters, which implies a self-amplifying $\lambda-\sigma$ relationship causes the particles to preferably deposit at small cake depths.

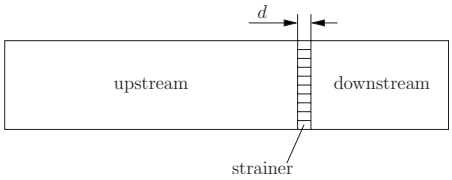

Fig. 10 Strainer represented as CFX subdomain

4 Implementation Into the CFD Code ANSYS-CFX

Equations (8), (14), and (12) for the clean fiber cake have been implemented into the CFD code ANSYS-CFX in order to calculate the transient build-up of the pressure drop over nonuniformly loaded strainers. This task is addressed by placing a subdomain of fixed thickness d into the flow geometry. It represents the filter cake and the strainer plate and separates the upstream from the downstream region, as illustrated in Fig. 10. The cross-stream distribution of the strainer resistance is made up by a parallel connection of multiple resistances, the magnitude of each depending on the local fiber mass load and superficial velocity values.

In order to make allowance for transient flows, the strainer mass load distribution at time t has to be calculated by integrating the fibrous particle phase mass flow passing through the strainer subdomain with respect to time according to

$$N_f(t) = \rho_f \int_0^t \zeta_f \mathbf{u}_f \cdot \mathbf{n} d\tau \tag{38}$$

where ζ_f represents the local fibrous particle phase volume fraction of the flow and $\mathbf{u}_f \cdot \mathbf{n}$ the velocity component of the fibers in the direction of the strainer normal $\mathbf{n}$.

The compacting pressure p_k acting on the strainer can be computed from the local values of fiber mass load N_f and superficial velocity U by solving Eqs. (8), (12), and (14). Superficial velocity U in Eq. (8) is obtained from liquid phase velocity $\mathbf{u}$ by

$$U = (1 - \zeta_f)\mathbf{u} \cdot \mathbf{n} \tag{39}$$

Again, the actual task of integrating the system of differential Eqs. (8) and (14) is passed on to the differential equation solver LSODAR. The wanted pressure drop Δp is readily obtained from the compaction pressure p_k according to Eq. (15).

Now, the flow resistance the liquid phase experiences within the strainer subdomain can be determined. It is modeled as source S in the momentum transport equation using the "isotropic loss model" of CFX

$$S = -(\alpha \mu u + \beta \rho u^2) \tag{40}$$

where α and β are the linear and quadratic loss coefficients. The computed pressure drop Δp already contains the viscous ($\propto u$) and inertial ($\propto u^2$) contributions to the momentum loss, cf. Eq. (7). Therefore, only one of the coefficients α or β needs to be determined, while the other can be set to zero. Here, the linear coefficient has been chosen. It reads

$$\alpha = \left| \frac{\Delta p}{\mu d \mathbf{u} \cdot \mathbf{n}} \right| \tag{41}$$

Momentum source (40) can now be set for the strainer subdomain. On solving the momentum equations in a CFX solver run, integration of Eq. (40) establishes the previously determined pressure drop between the up and downstream ends of the strainer subdomain.

For testing the implementation, a step like channel geometry with a horizontally embedded strainer was constructed. Together with a nonuniformly distributed fibrous particle phase in the inflow, this will lead to an unevenly loaded strainer. Details of the case definition can be found in Ref. [22].

Downloaded 02 Jun 2010 to 171.66.16.96. Redistribution subject to ASME license or copyright; see http://www.asme.org/terms/Terms_Use.cfm

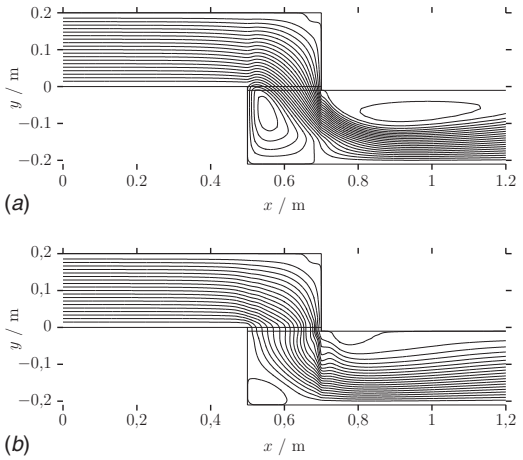

Fig. 11 Flow field (streamlines) in the channel mid plane; (*a*) $t=0$ s and (*b*) $t=40$ s

Flow fields at different simulation times are shown in Fig. 11. The solution at $t=0$ s corresponds to the stationary solution that was found for clear water filling the computational domain. A large recirculation area forms behind the back facing step in the lower channel section and two smaller ones at the upper right corner of the upstream section, as well as beneath the upper wall of the downstream section. The most noticeable difference between the flow fields at start and end of the simulation is the flow direction in the strainer subdomain. The particle laden strainer acts like a rectifier, which forces the flow into the vertical direction. This rectifying effect is caused by the high pressure drop over the clogged strainer leading to a pressure gradient, whose maximum is in the strainer normal direction. Throughout the simulation, a constant velocity of $u=4$ cm s^{-1} and a linear volume fraction profile of the fibrous particle phase with $\zeta_f=0$ at the channel top and $\zeta_f=0.015$ at the channel bottom were specified as inlet boundary conditions at $x=0$.

5 Conclusion

The linear relationship between superficial flow velocity and pressure drop, as suggested by Darcy's law, fails in the case of compressible fibrous media. In the present article a combination of a semi-empirical flow equation and a material equation is proposed that allows one to calculate the pressure drop in beds composed of this class of materials. The system of model equations constitutes an initial value problem, which is solved numerically for given strainer mass load and flow velocity. Solid density, mass specific surface, and the static compaction properties of the fibrous material need to be known.

Computed porosity and compaction pressure profiles are nonlinear along the fiber bed since they depend on each other. The experimentally found nonlinear relationship between flow velocity and pressure drop could be reproduced with sufficient accuracy using a one-dimensional implementation of the model equations.

The pressure drop model was extended to calculate the clogging of the initially clean fiber cake by particles removed from a suspension. Simple relations have been used to account for the dependency of the filter coefficient and of the pressure drop on the quantity of deposited material. However, the general applicability of the modeling framework could be demonstrated. Further experimental and modeling effort is necessary to enable it for practical applications.

The model has been successfully implemented as an extension to the general-purpose CFD code ANSYS-CFX. Its capability to simulate the transient pressure drop build-up at nonuniformly loaded strainers in arbitrary three-dimensional geometries has been demonstrated using a steplike flow geometry with a horizontally embedded strainer plate. It was shown that the pressure drop at the strainer has a rectifying effect on the flow.

Acknowledgment

This study was funded by the German Federal Ministry of Economy and Technology under the Grant Nos. 1501270 and 1501307.

Nomenclature

A_f = specific surface area of fibers
C, D = parameters of the material equation, Eq. (12)
F_1, F_2 = correction functions for the filter coefficient and the pressure drop of the clogged fiber bed
L = total streamwise fiber cake length
N_f = fiber mass load per strainer unit area
U = superficial liquid phase velocity
V_f = volume of fibers
V_p = volume of deposited particles
V_v = void volume of the clean fiber cake
V_{tot} = total volume of the fiber cake
a, a_0, b = coefficients of the Davies–Ergun equation, Eq. (7)
$\tilde{a}$, $\tilde{b}$ = parameter groups, Eq. (33)
b_{F1}, b_{F2} = empirical parameters in correction functions F_1 and F_2, Eq. (37)
b_λ = empirical parameter in Eq. (35)
d = streamwise extension of CFX subdomain "strainer"
$\mathbf{n}$ = strainer normal vector
Δp = pressure drop
p_k = compaction pressure
t = time
$\mathbf{u}$ = liquid phase velocity vector
u = particle suspension approach velocity
up (subscript) = value at upstream end of fiber cake
x = space coordinate
x_{pen} = penetration depth of particle suspension
′ (superscript) = related value in the uncompressed fiber bed
α and β = linear and quadratic loss coefficients
ε = clean fiber cake porosity
ε_0 and ε_∞ = fiber cake porosities at zero and infinite compaction pressures
λ and λ_c = filter coefficient and clean fiber cake filter coefficient
μ = liquid phase dynamic viscosity
ρ_f = material density of fibers
ρ = liquid phase density
σ = volumetric deposit
ζ_p = particle suspension concentration

References

[1] OECD NEA, 1995, "Knowledge Base for Emergency Core Cooling System Recirculation Reliability," NEA/CSNI/R(1995)11.
[2] NRC, 2003, "Knowledge Base for the Effect of Debris on Pressurized Water Reactor Emergency Core Cooling Sump Performance," NUREG/CR-6808.
[3] OECD NEA, 2004, "Debris Impact on Emergency Coolant Recirculation," Workshop Proceedings, Albuquerque, NM.
[4] ENS, 1992, "Swedish N-Utilities Explain BWR Emergency Core Cooling Problem," ENS Nuclear News Network, No. 358/92.
[5] NRC, , "Small-Scale Experiments: Effects of Chemical Reactions on Debris-Bed Head Loss," NUREG/CR-6868.
[6] ANSYS Inc., 2008, ANSYS CFX, http://www.ansys.com/products/cfx
[7] Andrade, J. S., Jr., Costa, U. M. S., Almeida, M. P., Makse, H. A., and Stanley, H. E., 1999, "Inertial Effects on Fluid Flow Through Disordered Porous Media," Phys. Rev. Lett., **82**, pp. 5249–5252.
[8] Dullien, F. A. L., 1979, *Porous Media Fluid Transport and Pore Structure*, Academic, New York.

Downloaded 02 Jun 2010 to 171.66.16.96. Redistribution subject to ASME license or copyright; see http://www.asme.org/terms/Terms_Use.cfm

[9] Carman, P. C., 1937, "Fluid Flow Through Granular Beds," Trans. Inst. Chem. Eng., **15a**, pp. 150–166.
[10] Kyan, C., Wasan, D. T., and Kintner, R. C., 1970, "Flow of Single-Phase Fluids Through Fibrous Beds," Ind. Eng. Chem. Fundam., **9**, pp. 596–603.
[11] Davies, C. N., 1952, "The Separation of Airborne Dust and Particles," Proc. Inst. Mech. Eng., **1B**, pp. 185–198.
[12] Ingmanson, W. L., Andrews, B. D., and Johnson, R. C., 1959, "Internal Pressure Distributions in Compressible Mats under Fluid Stress," Tappi J., **42**, pp. 840–849.
[13] Ergun, S., 1952, "Fluid Flow Through Packed Columns," Chem. Eng. Prog., **48**, pp. 89–94.
[14] Jönsson, K. A.-S., and Jönsson, B. T. L., 1992, "Fluid Flow in Compressible Porous Media: I: Steady-State Conditions," AIChE J., **38**, pp. 1340–1348.
[15] Meyer, H., 1962, "A Filtration Theory for Compressible Fibrous Beds Formed From Dilute Suspensions," Tappi J., **45**, pp. 296–310.
[16] Williams, T., et al., 2008, GNUPLOT, http://www.gnuplot.info
[17] Herzig, J. P., Leclerc, D. M., and Le Goff, P., 1970, "Flow of Suspensions Through Porous Media—Application to Deep Filtration," Ind. Eng. Chem., **62**, pp. 8–35.
[18] Tien, C., and Payatakes, A. C., 1979, "Advances in Deep Bed Filtration," AIChE J., **25**, pp. 737–759.
[19] Hindmarsh, A., et al., 2008, ODEPACK, http://www.netlib.org/odepack
[20] Jegatheesan, V., and Vigneswaran, S., 2005, "Deep Bed Filtration: Mathematical Models and Observations," Crit. Rev. Environ. Sci. Technol., **35**, pp. 515–569.
[21] Bai, R., and Mackie, R. I., 1995, "Modelling the Transition Between Deposition Modes in Deep Bed Filtration," Water Res., **29**, pp. 2601–2604.
[22] Grahn, A., Krepper, E., Alt, S., and Kästner, W., 2008, "Implementation of a Strainer Model for Calculating the Pressure Drop Across Beds of Compressible, Fibrous Materials," Nucl. Eng. Des., **238**, pp. 2546–2553.

Downloaded 02 Jun 2010 to 171.66.16.96. Redistribution subject to ASME license or copyright; see http://www.asme.org/terms/Terms_Use.cfm